Express Polymer Letters Vol.17, No.11 (2023) 1135–1153
Available online at www.expresspolymlett.com
https://doi.org/10.3144/expresspolymlett.2023.86

Research article

A comparison of the mechanical behaviour of natural rubber-based blends using waste rubber particles obtained by cryogrinding and high-shear mixing

Nicolas Candau[*], *Rachel LeBlanc, Maria Lluisa Maspoch*

Departament de Ciència i Enginyeria de Materials (CEM), Escola d'Enginyeria Barcelona-Est (EEBE), Universitat Politècnica de Catalunya BARCELONATECH (UPC)- Av. Eduard Maristany 16, 08019 Barcelona, Spain

Received 24 June 2023; accepted in revised form 25 July 2023

Abstract. The influence of the type of mechanical recycling of waste rubber particles on the tensile properties of waste/natural rubber blends has been investigated. The wastes originating from ground tyre rubber (GTR) had been treated by two distinct processes: cryo-grinding and high shear mixing (HSM). For both processes, the resulting composites show enhanced stiffness and strength for all strain rates and temperatures tested. This is attributed to both the reinforcing effect of the waste as well as the nucleation ability of the wastes on strain induced crystallization (SIC) in the natural rubber (NR) matrix. Cryo-grinding was shown to provide the finest particle size with an average diameter of 34 μm, while the HSM process was found to show an elastic modulus of aggregated GTR powder of 7 MPa at 1 Hz at room temperature. Within these characteristics, the NR/GTR blends using the HSM process show the best tensile performance under single loading, with the highest strength and highest ability to crystallize under strain. Under cyclic loading, NR/GTR blends using cryo-ground GTR particles show the best performance, which we ascribed to their ability to better distribute and accommodate the stress from one cycle to another owing to their finest size. Both explored recycling techniques provide the natural/waste rubber blends interesting properties such as mechanical reinforcement and strain-induced crystallization ability under various testing conditions.

Keywords: *natural rubber, recycling of rubbers, revulcanization, waste testing, tensile testing, strain induced crystallization*

1. Introduction

With a growing concern about the environmental impact of waste and the need to conserve resources, there is an increasing interest in recycling and reusing polymeric materials, such as plastics and rubbers [1]. In recent years, there has been significant progress in developing technologies and processes for recycling rubber in line with the 2030 Sustainable Development Goals (SDGs) and the 2050 European Green Deal. These processes can potentially recover valuable materials from waste rubber and reduce the amount of waste accumulated in landfills and oceans [2]. The demand for recycled rubber products is also increasing as companies and consumers seek more sustainable alternatives to virgin rubber [3], including the construction, automotive, sports, and footwear industries. However, there are still challenges to overcome in rubber recycling, such as technical limitations or cost-effectiveness.

The main recycling methods for rubbers include (i) mechanical recycling, which involves shredding or grinding of rubber waste into small pieces [4], (ii) chemical recycling which involves breaking down the rubber waste into its constituent chemicals using chemical processes, such as depolymerization [5], (iii) devulcanization that is the process of breaking the chemical cross-links that provides to rubber its elasticity, making it possible to reuse the material

[*]Corresponding author, e-mail: nicolas.candau@upc.edu

[6], (iv) pyrolysis that is a thermal decomposition process that breaks down waste rubber into smaller molecules in the absence of oxygen, producing gases, oils, and carbon black [7]. While there may be some energy and resource inputs associated with the grinding or shredding process, mechanical processes are generally considered to be one of the more environmentally friendly options for rubber recycling, as it does not involve the use of chemicals and usually do not generate toxins. Among these mechanical methods, cryo-grinding and high shear mixing are promising processes to obtain residues with high added values.

Cryogrinding involves using liquid nitrogen or other cryogenic gases to cool the material being ground to very low temperatures. The material is then ground using types of equipment such as cryo-mills, which operate at very high speeds to reduce the size of the waste particles. Cryogrinding can produce particles with a narrow size distribution and a fine particle size [8], especially compared to ambient grinding [9]. High shear mixing involves the application of mechanical forces onto materials to achieve mixing, dispersion, or emulsification. This can be carried out using equipment such as rotor-stator mixers, high-pressure homogenizers, or colloid mills. The resulting products can have a homogeneous texture and fine particle size distribution. High shear mixing is a more complex and expensive process compared to traditional grinding, but it can offer greater control over the final product properties [10].

The waste rubber originated from the treatment of pneumatic tyres (so-called ground tyre rubber), and can be re-compounded without any addition of other raw material, showing high mechanical resistance but low strain at break (around 200%) [11]. To get materials with high deformability and/or toughness, providing them sufficient properties for novel application with high added value, the waste rubber can be blended with polymeric matrices, such as fresh plastic, thermoset rubber matrices [12] or concrete [13]. Among these materials, natural rubber (NR) is an interesting candidate to be used as the rubber matrix owing its excellent large strain properties such as fatigue behaviour, strain-induced crystallization ability as well as its compatibility with the waste rubber from the pneumatic tires as the latter contains vulcanized (and/or partially devulcanized) natural rubber.

The incorporation of waste rubber as reinforcing filler has been used as a strategy to improve the tensile properties of NR. The tensile strength and modulus of the waste/natural rubber blends usually increase while the elongation at break decreases [14]. Moreover, it has been shown that the reinforcement efficiency of traditional fillers, such as carbon black and silica, can sometimes be improved by substituting them with waste fillers [15]. The thermal and dynamic mechanical properties of waste rubber/natural rubber blends demonstrate that the resulting composites containing a natural rubber matrix and waste rubber as fillers show excellent damping behaviour [16]. Finally, the use of waste rubber in natural rubber matrices has been shown to reduce the environmental impact and carbon footprint compared to traditional rubber materials [15].

As mentioned above, strain-induced crystallization (SIC) in NR is one crucial factor that has been considered in recent studies dedicated to the design of waste/natural rubber blends. SIC is a phenomenon in which the application of deformation to natural rubber leads to the alignment of polymer chains and the formation of crystalline domains, resulting in improved mechanical properties (large strain reinforcement and increased fatigue life). Incorporating waste rubber into the natural rubber matrix can positively affect SIC, as has been shown recently by *in-situ* X-rays [17] and *in-situ* IR thermography [18, 19]. Nonetheless, none of these studies focused on the possible effect of the type of treatment applied to the wastes (devulcanization, grinding, *etc*.), while they are expected to result in a drastic modification of the ultimate properties of the waste/rubber blend.

In this paper, we prepared waste/natural rubber blends using two distinct mechanical waste treatments: the cryo-grinding process and the high-shear mixing process. The properties of the wastes, as well as the tensile properties of the resulting waste/natural rubber composites, are discussed, and a focus is done on the impact of the type of waste treatment on the large strain reinforcement of the blends.

2. Materials and experiments

2.1. Materials processing

Natural rubber (NR) is a Standard Malaysian Rubber (SMR, Akrochem company, Akron, USA). It has a CV60 of about 55–60 (Mooney viscosity ML 1 + 4, 100 °C:). It contains 0.15% of hydroxylamine that had been added to the latex stage to prevent the raw rubber from stiffening while storing. Ground tire rubber (GTR, J. Allcock & Sons Ltd Company, Manchester,

United Kingdom). Tire buffing was used to transform the rubber from the pneumatic tire into millimeter size crumbs. Two types of particles were obtained using a cryogrinding process or a high-shear mixing process (HSM, REP-International company, Corbas, France), as indicated in Table 1.

The crumbs, size-reduced via a controlled cryogrinding, are free of contaminants such as textile, metal, and road dirt. Nonetheless, they look grey as talc had to be added to make the material flow and sieve correctly during the cryogrinding process. The cryoground GTR ($GTR_{(d)}$) was subsequently sieved using a vibratory sieve shaker (Analysette 3, Fritsch GmbH, Idar-Oberstein, Germany) with a mesh 230's (size <63 μm).

The high shear mixing process consists of two metallic cones (a stator and a rotor) with a series of grooves on their surfaces were used. The distance between the surfaces of both cones (gap) was optimized to provide the finest waste particle sizes. The rotation speed and the direction of rotation make the rubber move into the grooves of the cones, stressing and relaxing in a continuous and rapid way. Based on the geometry of the cones, the material is highly sheared when the material is located between the zenith flat parts. Three sequences of 5 min were applied to the waste rubber to avoid continuous processing and hence limit the self-heating that may cause thermal degradation and/or re-vulcanization *in situ*. The crumbs obtained from HSM ($GTR_{(h)}$) were subsequently sieved using a vibratory sieve shaker (Analysette 3, FRITSCH Bakery Technologies GmbH & Co. KG, Germany) with a mesh 120's (size <125 μm).

To prepare the NR/GTR blends, the NR was first masticated inside the chamber of an internal mixer (Brabender Plastic-Corder W50EHT, Brabender GmbH & Co., Duisburg, Germany) at a temperature of 80 °C, for 5 min and a rotation speed of 40 rpm. 5 more minutes the vulcanizing agent dicumyl peroxide (DCP, Thermo Fisher Scientific, Waltham, Massachusetts, USA) was added (see Table 1) and mixed for 5 min. The masterbatch containing NR, GTR and DCP was vulcanized according to the estimated optimal time at 170 °C under 4 MPa. The curing curves were recorded by using a Moving Die Rheometer (Monsanto moving die rheometer MDR 2000E, MonTech, Columbia City, USA) oscillating at a constant frequency of 1.677 Hz and an amplitude of deformation of 1.38% (5°) at the vulcanization temperature (166–171 °C). To perform the tensile tests, dogbone-shaped specimens with a 1 mm thickness, 4 mm width and 15 mm length were extracted from hot moulded sheets by die-cutting with a specimen preparation punching machine (Manual Hollow Die Punch, CEAST company, Torino, Italy).

Table 1. Materials codes. The mesh size indicates the size of the sieving used to extract the GTR that is further used to prepare the NR/GTR blends.

Material code	GTR [wt%]	Mesh size*	Curing *T* [°C]	DCP** [wt%]	DCP/NR*** [wt%]
$GTR_{(g)}$	100	230's	×	×	×
$GTR_{(h)}$	100	120's	×	×	×
NR	0	×	170	1.50	1.50
$NR/GTR_{(g–)}$	20	230's	170	1.30	1.50
$NR/GTR_{(g+)}$	20	230's	170	1.63	1.88
$NR/GTR_{(h–)}$	20	120's	170	1.30	1.50
$NR/GTR_{(h+)}$	20	120's	170	1.63	1.88

*Values are based on the American National Standard for Industrial Wire Cloth (American Standard ASTM-E 11.

**The DCP was introduced as a weight percent of the overall rubber phase quantity *i.e.*, the NR phase in the case of vulcanized NR and the NR phase + rubber phase in the GTR in the case of the vulcanized NR/GTR blends.

***The DCP calculated as a function of the NR content only.

2.2. Dynamic mechanical analysis

Dynamic mechanical analysis (DMA) was performed on rectangular samples using DMA equipment (Q800, TA Instruments, New Castle, USA). Specimens were tested in tension mode using pre-stress of 1 N, an amplitude of cyclic deformation of 0.5%, and a frequency varying from 1 to 100 Hz (frequency sweep method). The temperature was maintained at 25 °C.

2.3. Fourier-transform infrared spectroscopy

Fourier-transform infrared spectroscopy (FTIR) was performed at room temperature (25 °C). Absorbance spectra were recorded on an FTIR spectrometer (Nicolet 6700 FTIR, Thermo Scientific, Waltham, Massachusetts, USA) equipped with Cesium Iodide (CsI) beamsplitter to measure in attenuated total reflection modes. Spectra were obtained in the wavenumber interval ranging from 600 to 4000 cm^{-1}.

2.4. Swelling

The rubber was immersed in cyclohexane (Cyclohexane, ACS, 99+%, Thermo Scientific Chemicals, Waltham, Massachusetts, USA) for 72 h. After 72 h the swollen mass was measured. The rubber was then placed under a hood at room temperature for 72 h to

remove the solvent. The mass of the dry samples was then measured. The average network chain density has been calculated from swelling experiments and the Flory-Rehner equation (Equation 1) [20]:

$$v = \frac{\ln(1-v_2) + v_2 + \chi_1 v_2^2}{V_1\left(-v_2^{\frac{1}{3}} + \frac{2}{f}v_2\right)} \quad (1)$$

where V_1 = 108 cm^3/mol is the molar volume of the solvent (cyclohexane), χ_1 is the Flory-Huggins polymer solvent dimensionless interaction term (χ_1 is the Flory-Huggins polymer solvent dimensionless interaction term and is equal to 0.363 in the case of NR-cyclohexane [21]). $v_2 = 1/Q_r$, with Q_r the swelling ratio of the rubber matrix. $Q_r = V/V_0$ where V and V_0 are the volumes of the rubber network, at swelling equilibrium and after swelling and drying respectively. The ratio $2/f$ is associated with the phantom model that assumes spatial fluctuation of crosslinks (non-affine) used for high deformation ratios. f, the crosslink functionality, is chosen equal to 4. For filled compounds the Kraus correction [22] is used to account for the contribution of filler in the swelling ratio (Equation (2)):

$$Q_r = \frac{Q_c - \varphi}{1 - \varphi} \quad (2)$$

with φ is the volume fraction of fillers, and Q_c the swelling ratio of the composite. Equation (2) assumes non-adhesion of the fillers to the rubbery matrix, hence creating vacuoles in the swollen state.

2.5. Thermogravimetry analysis

Thermogravimetric analysis (TGA) is performed on GTR particles and on NR/GTR blends (DSC 1 Star System, Mettler Toledo, Columbus, OH, USA). The materials are put into an alumina crucible with a quantity of around 5–10 mg. The standard IEC 60811-100 is used for the determination of the carbon black content. To do so, the GTR is heated from 30 to 1000 °C with a heating ramp of 10 °C/min working under a nitrogen environment from 30 to 850 °C, and under an air environment from 850 to 1000 °C.

2.6. Micro-computed tomography (µCT)

3D morphological information of rubber blends was obtained by micro-computed X-ray tomography (µCT) carried out on a microtomograph Skyscan 1272 by Bruker (Billerica, Massachusetts, USA) equipped with an X-ray generator of 10 W, 20–100 kV, an X-ray detector of 11 MP (4032×2688 pixels), with a maximum resolution of 0.45 µm. The volume-of-interest (VOI) was chosen around 7–13 mm^3. An acceleration voltage of 50 kV at a current of 200 µA was employed. A full rotation (360°) was used with projections taken every 0.25°. The source-to-object-distance (SOD) and source-to-detector-distance (SDD) were set to obtain a voxel size of 3 µm. The 3D volume reconstruction of the projections was generated by Bruker software. Image treatment and analysis were performed with the commercial software Avizo (Thermo Fisher Scientific Inc., USA). The inherent noise of the acquired images was reduced by means of a median filter. Finally, images were binarized by thresholding the grayscale histogram.

2.7. Uniaxial tensile tests and uniaxial cyclic tests

Uniaxial tests were performed on a universal testing machine equipped with a 5 kN force sensor (Z008 Zwick/Roell, Ars Laquenexy, France). The first test type consists of a uniaxial stretching up to failure at a constant crosshead speed and temperature. Several conditions have been tested, with a crosshead speed varying from 100 to 2000 mm/min, corresponding to a nominal strain rate of 1.1 and 222 %/s, respectively, according to the specimen dimensions (15 mm length), and a temperature varying from –25 to 80 °C. The second type of test is an incremental test performed at a constant crosshead speed and at room temperature that consists of the application of a series of cycles, with an increment of the maximum deformation reached during cycles (from 50% for the first cycles to 500% for the last cycles). The test generally stops due to specimen breakage. At each applied cycle, the specimen is unloaded until reaching the relaxed state (zero force). The third type of test is a cyclic test performed at a constant frequency of 0.3 Hz. The strain amplitude of the cycles is chosen to equal 200%, which means a nominal strain rate of 120 %/s. Before the cyclic deformation, the rubber specimen is pre-deformed up to 400%. The cyclic tests start with an unloading and then a loading, meaning that the cyclic tests are performed between the deformation of 200 and 400%. For each type of test, the specimen deformation was estimated by measuring the local displacement between two white lines drawn in the central part of the specimen, separated by an initial distance of 10 mm and orthogonal to the specimen tensile axis. The local

Table 2. Testing conditions for the three types of tests: tensile test, incremental test, and cyclic test.

Type of test	Nominal strain rate [%/s]	Temperature [°C]	Cyclic deformation [%]	Pre-deformation [%]
Tensile test	1.1	21	×	×
	11	21	×	×
	56	21	×	×
	222	21	×	×
	11	–25	×	×
	11	80	×	×
Incremental test	11	21	Incremental*	×
Cyclic test	120	21	200	400**

*During the incremental tests, the maximum loading is increased from 50 to 500%, with an increment of around 30–35%. Each cycle is performed with an unloading down to zero force.

**During the cyclic test, after the pre-deformation at 400% the cycles start with an unloading followed by a loading, *i.e.*, the cycle occurs between 200 and 400%.

strain rate accounting for this correction has been estimated and found to decrease slightly with applied strain. A summary of the testing conditions for the three types of tests is shown in Table 2.

3. Results and discussion

3.1. Characterization of the waste rubber and waste rubber-based blends

Prior to the preparation of the natural rubber/ground tyre rubber blends, the GTR waste from the same batch was passed through two distinct processes: cryo-grinding or high shear mixing (HSM). The wastes obtained after these processes were sieved to collect the smallest rubber particles. The GTR particles were subsequently siegved. As cryo-grinding usually results in quite small particles, it was possible to collect enough $GTR_{(d)}$ particles with a mesh 120's (size <63 μm) to prepare the blends. Contrarily, the $GTR_{(h)}$ crumbs obtained from HSM could have been collected in sufficient quantity only by using the sieving size <125 μm. To quantify their average size and their size distribution by μCT, the GTR particles were dispersed into an NR matrix at 5 wt%, a content sufficiently low to allow the analysis on isolated GTR particles (Figure 1a). The 2D representative tomography images of the resulting NR/GTR composites (Figures 1a and 1b) show different intensities of grey due to the density contrast of the phases. The whitest grey is ascribed to the waste particles, being denser owing to their high content in carbon black, and the continuous phase, namely the NR matrix, is represented by the darkest grey regions. White domains had been observed that represent some highly dense particles (talc from grinding, traces of zinc oxide originating from the sulphur vulcanization of the tire). A filter size has been applied to remove their contribution. Quantitative observations reveal that the size distribution of the $GTR_{(g)}$ is quite homogeneous compared to the size distribution of the $GTR_{(h)}$. One may note that the largest sizes of $GTR_{(h)}$ and $GTR_{(g)}$ are found to be higher than the sieving size. This might be explained by the high aspect ratio of certain GTR particles that are sieved. The average size of the $GTR_{(g)}$ and $GTR_{(h)}$ are found to be equal to 34 and 83 μm, respectively. By making an analysis of isolated GTR particles, it has been found that the specific surface (object surface/volume ratio) was equal to 84 and 37 mm^{-1} for cryoground GTR and GTR obtained by HSM.

While the $GTR_{(h)}$ particles show some limited size reduction as compared to the $GTR_{(d)}$, the HSM process has been carried out with the aim of selectively breaking the covalent bonds (devulcanization), through the application of high shear forces. Such devulcanization is expected to occur in the whole volume of the GTR particles, as shown in Figure 1c. However, the GTR surface is more easily exposed to a further reaction with another phase (in our case, the NR matrix) during their blending and re-vulcanization in the presence of a new vulcanizing agent (in our case, the dicumyl peroxide). To investigate the reactivity of the $GTR_{(h)}$ particles, we prepared three systems: a GTR powder without vulcanization agent, an NR, and an NR/GTR blend with a vulcanization agent (1.5 wt% of the NR phase). We cured all of them at 170 °C for 10 minutes by using a moving die rheometer (MDR) to track the evolution of the torque with time, indicative of the formation of crosslinks (Figure 2). Interestingly, from the naked eye's observation, the cured powder of GTR showed certain cohesion, suggesting the formation of possible interfacial bonds between the GTR particles.

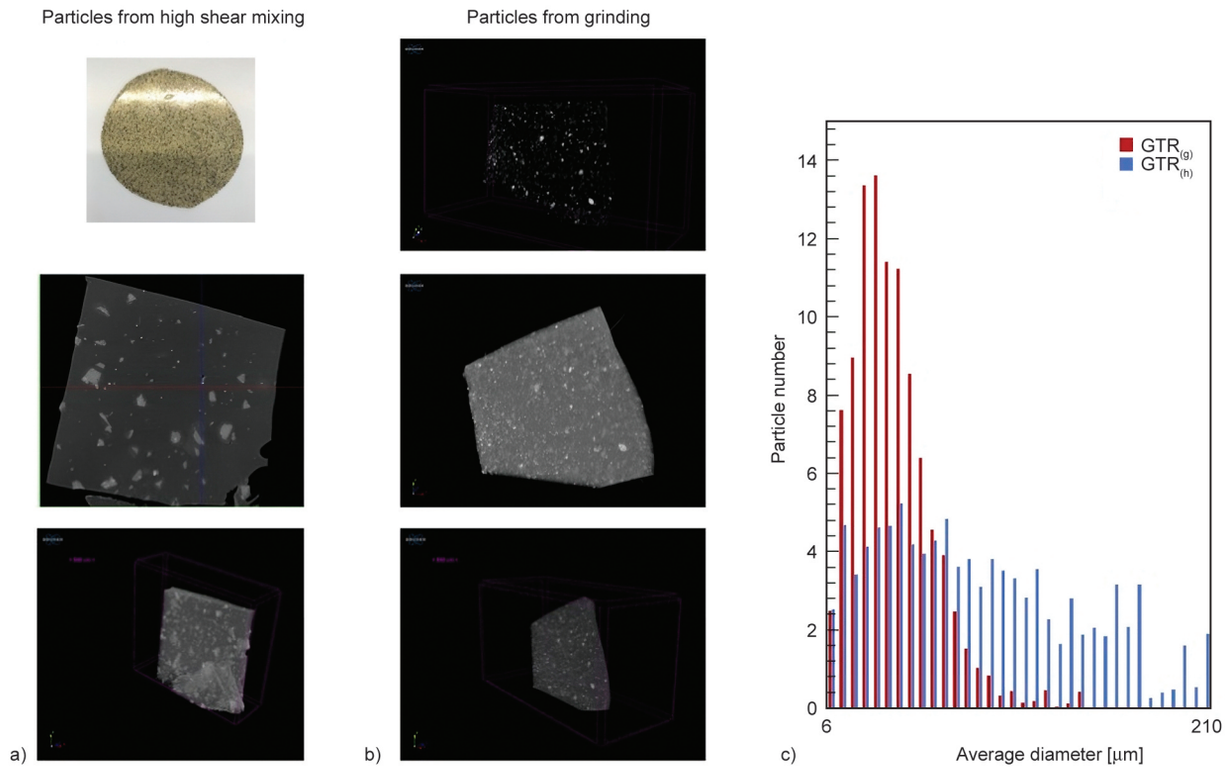

Figure 1. a) $GTR_{(h)}$ and b) $GTR_{(g)}$ particles obtained from the high shear mixing process and cryo-grinding process, respectively. µCT was performed on NR/GTR blends containing 5 wt% of GTR to avoid possible aggregation for the GTR. c) GTR particle size distribution in number. The representative volumes of observations (represented in violet lines) correspond to approximate volumes of 7–13 mm^3.

This statement is consistent with increased torque with time suggesting the formation of crosslinks of the resulting bulk powder (Figure 2a). This may originate from the vulcanization of the wastes by two possible concomitant mechanisms: (i) the activation of a residual sulphur vulcanization system persisting after the curing process of the pneumatic tyre and/or (ii) the re-activation of sulphur bonds broken after application of the high shear mixing process. Both the NR and NR/GTR blends show an increase of torque with curing time, confirming crosslinking reactions again. The minimum and maximum torque is logically found to increase with the addition of wastes, as they act, owing to their carbon black content, as reinforcing particles, in both unvulcanized and vulcanized states.

In filled rubber, the torque increase is larger, and the proportionality of the crosslink density to the torque increase is no longer true in the case of filled compounds since the contribution of fillers to the viscosity is higher in the vulcanized state [23, 24].

Nonetheless, the increment of the torque (Figure 2b) is found to be significantly higher in the NR/GTR blend (relative increment of 350%), compared to the NR (relative increment of 280%), and to the GTR powder (relative increment of 26%). This suggests a higher reactivity in terms of crosslink creation. This may arise from the creation of supplementary bonds at the interface between the GTR particles and the NR matrix, resulting in the fixation of the GTR to the NR matrix, hence increasing the viscosity of the blend and hence the torque increment.

Given these previous rheological results, the effect of the GTR distribution, as well as their reactivity with the NR matrix, that results in both waste treatments and blends vulcanization, are also expected to have an impact on the small and large strain mechanical properties. This will be studied in the following.

Dynamic mechanical analysis (DMA) experiments were performed on the bulk powder GTR cured for 10 minutes at 170 °C and compared with the DMA response of the NR matrix cured in the same conditions (Figure 3) to further demonstrate the elastic response of the GTR bulk powder. Not only the aggregated GTR show cohesion, as previously observed, but they also show a small strain elastic response, with an elastic modulus increasing linearly from 7 to 11 MPa in the frequency range of 1–100 Hz. This result confirms the creation of interfacial bonds elastically active at the GTR surface, consistent with the

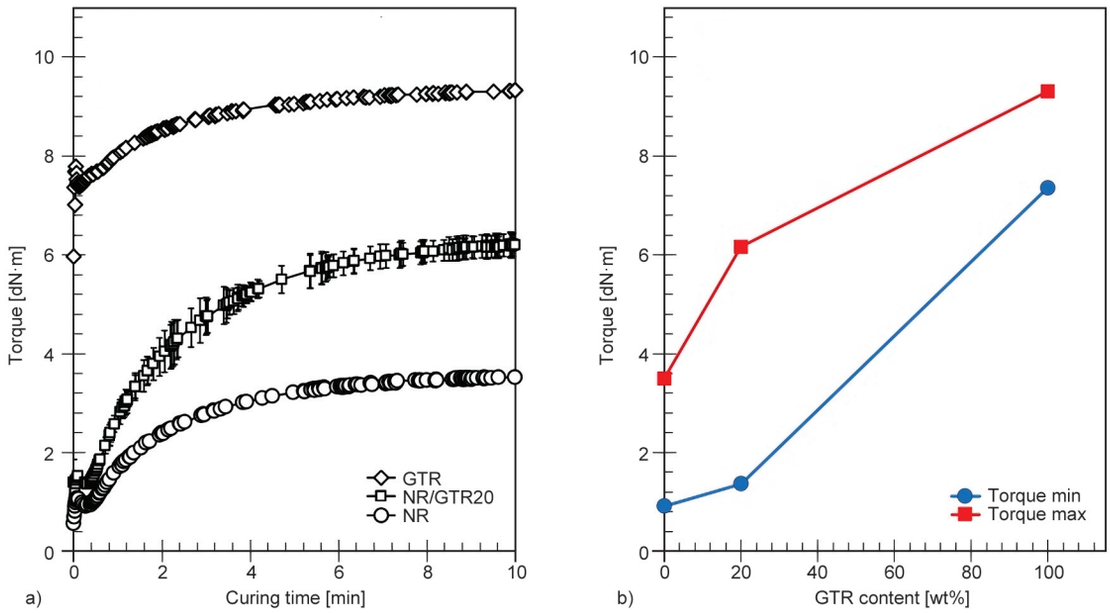

Figure 2. a) Torque *versus* curing time by using moving die rheometry (MDR) technique, performed on natural rubber matrix (NR), $GTR_{(h)}$ powder obtained after the HSM process (see experimental section) and on NR/$GTR_{(h)}$ material (see Table 1 for the materials nomenclature). b) Maximum and minimum torque during the MDR experiment.

torque increase in previously described rheology experiments.

Before further investigating the large strain response of the NR/GTR blends, as well as the reinforcing effect of the various phases (*e.g.*, rubber phase and carbon black (CB) present in the GTR), it is important to identify their fraction. Thermogravimetric Analysis (TGA) may be used to solve it. Most of the rubber is expected to decompose below 500 °C as sown on the TGA curves (Figure 4). It has been shown in the literature that the formation of short hydrocarbons attests to the thermal degradation of the rubber chains above 500 °C [25]. The remaining materials above 500 °C attest to the presence of non-rubber components, most likely CB aggregates and eventually, in a few proportions, some clay minerals that can arise from the application of the cryo-grinding process (see experimental section) for the series of materials based on $HSM_{(g)}$. The mass loss of the NR matrix (Figure 4a) shows a single decomposition process with a maximum at around 350 °C, that corresponds to the degradation of the polyisoprene chains. The GTR particles show a distinct decomposition process: the degradation of the rubber phase is delayed as compared to the one of the NR, that is due to the presence of Styrene Butadiene Rubber (SBR) in the GTR with a higher decomposition temperature (around 430 °C). The material remaining at 500 °C corresponds to the non-rubber components. It mostly corresponds to the CB fraction, of similar quantity between $GTR_{(h)}$ and $GTR_{(g)}$, as both types of waste come from the same batch. Few amounts of talc used for the cryo-grinding process, which decomposes at temperatures close to 900 °C [26], may contribute to the total weight. This explains why the mass loss is slightly higher in $GTR_{(g)}$ compared to $GTR_{(h)}$ after rubber degradation. Figure 4b, 4c shows the thermal decomposition of NR/GTR blends as

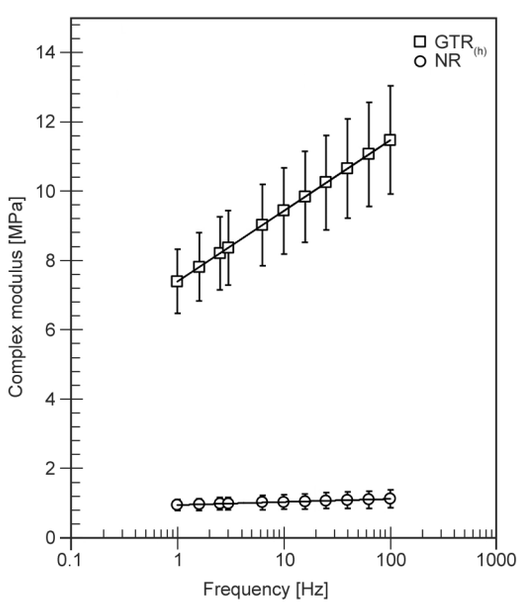

Figure 3. Complex modulus [MPa] *versus* frequency [Hz] (in log scale) for NR and $GTR_{(h)}$ materials between 1 and 100 Hz at 0.5% of deformation.

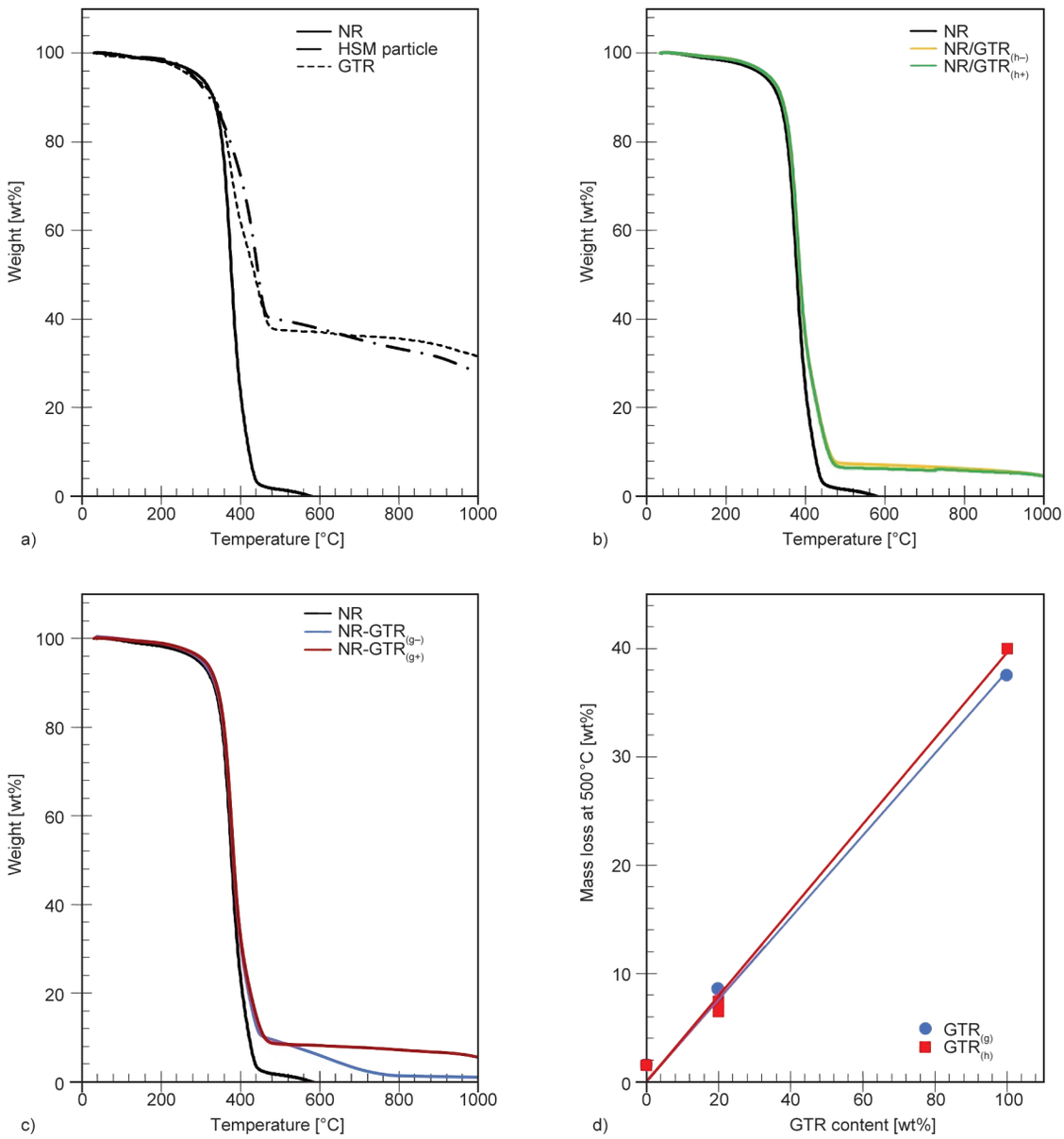

Figure 4. a), b), c) Thermogravimetric analysis curves of the various materials listed in Table 1. d) Mass loss at 500 °C *versus* the GTR content for the same series of materials.

compared to NR, highlighting the contribution of non-rubber components to be around 7–8 wt% at 500 °C. The remaining mass at 500 °C ascribed to non-rubber content expectedly follows a linear trend *versus* GTR content (Figure 4d). The GTR particles contain, on average, a total of 40 wt% of non-rubber elements. As the GTR represents the 20 wt% of the NR/GTR blends, this means that the non-rubber components occupy a total of 7–8 wt% in the NR/GTR blends.

An analysis of the chemical composition of the GTR and of the NR and NR/GTR blends, complementary to TGA, has been achieved by performing a Fourier transformed infrared spectroscopy (FTIR) (Figure 5). The 1500–800 cm^{-1} region includes the absorbance bands of elastomeric components and non-elastomeric components (SiO_2 or carbon black). The peak at 698 cm^{-1} corresponds to the $(C–H)_{op}$ bend of the mono-substituted benzene in the styrene butadiene rubber (SBR), present in the $GTR_{(g)}$ but hardly visible in the $GTR_{(h)}$. The peak at 830 cm^{-1} corresponds to the =C–H out of plane bending in rubber molecules [29]. Natural rubber cis-isomer configurations can be observed at 870–780 cm^{-1} for all materials [30] and the peak at 1375 cm^{-1} corresponds to the (C–H) symmetric bend of the-CH_3 bond in NR [31]. The peak at 1450 cm^{-1} corresponds to the $–CH_2–$ stretching of the elastomeric phases:

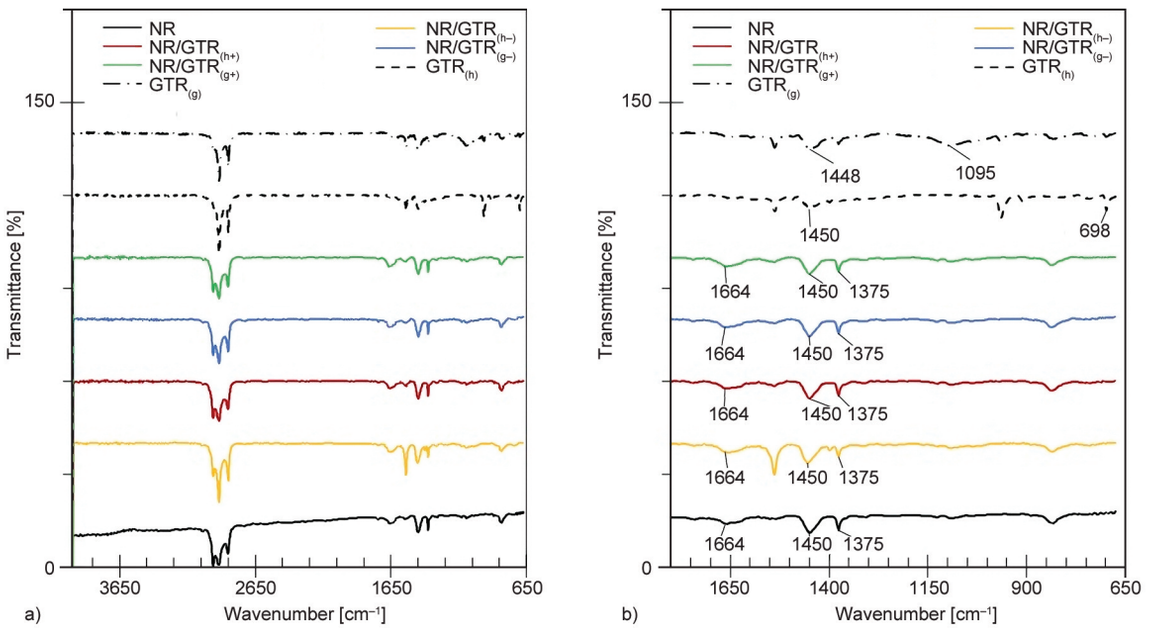

Figure 5. FTIR spectra from 650 to 4000 cm^{-1} of the $GTR_{(h)}$, $GTR_{(g)}$, and the different NR/GTR blends of the study. The curves had been shifted in the y-axis for the sake of clarity. a) full wavenumber range, b) selected wavenumber range between 650 and 1800 cm^{-1}.

NR molecules in the NR matrix and NR+SBR molecules in the GTR. The associated peak in the GTR is hence more intense as compared to the $–CH_3$ (C–H) symmetric bend. All the FTIR spectra show strong bands in the range of 3015–2744 cm^{-1}, indicative of the asymmetric and symmetric stretching frequency of the C–H groups (C–CH_3 and –CH_2–). The peak at 1095 cm^{-1} observed in the $GTR_{(g)}$ may correspond to the Si–O stretching due to the presence of talc used for the grinding process, consistent with TGA results (Figure 5). When comparing the FTIR of the NR/GTR vulcanized with various amount of DCP, the C=C stretch (1664 cm^{-1}) was not significantly different in all cases. In has been suggested in the literature, in that case, a predominance of an abstraction route over a radical addition in the peroxide vulcanization of NR at 170 °C [29].

One may note here that the crosslinking agent, DCP, has been introduced at two distinct contents (+ or –) to account for the following assumption: all rubber phases, *i.e.*, NR matrix and rubber contained into the GTR particles, may react with the DCP. Within this assumption, the DCP content is chosen equal to 1.30 and 1.63 wt%, respectively. If, however, it is assumed that only the NR phase reacts (and the rubber phase in the GTR reacts only at the waste surface), the percentages of DCP are found equal to 1.5 and 1.88 wt% of the NR matrix (cf. Table 1).

The volume percent of CB was calculated using a density of 1.9 $g \cdot mol^{-1}$. The network chain density, ν, was calculated following a simple rule of the mixture and from the knowledge of the density and weight fraction of the rubber phase and CB particles (see Equations (1), (2) in the experimental section). One may note that, even if a non-extended study has been carried out about the devulcanization state of the wastes, in a previous publication [28], we showed that the cryoground GTR with size <63 µm were found around 1.3 $mol \cdot cm^{-3}$.

The network chain density is found around $1.35 \cdot 10^{-4}$ $mol \cdot cm^{-3}$ in the case of the vulcanized NR (Figure 6), a network chain density close to the one of the cryoground GTR. Both the $NR/GTR_{(g–)}$ and $NR/GTR_{(h–)}$ have lower network chain density as compared to one of the NR. This may be explained by (i) the reaction of the rubber phase in the GTR particles with DCP that impedes efficient peroxide-vulcanization of the NR matrix and/or (ii) the concomitancy of both DCP degradation and sulphur reaction that may reduce the final crosslink density, as 1 mol of sulphur destroys 1 mol of DCP [27].

By increasing the quantity of DCP, the network chain density of the NR/GTR blend is found to increase from $1.1 \cdot 10^{-4}$ to $2.15 \cdot 10^{-4}$ $mol \cdot cm^{-3}$. This drastic change in crosslink density may suggest a better reactivity of the GTR particles with DCP

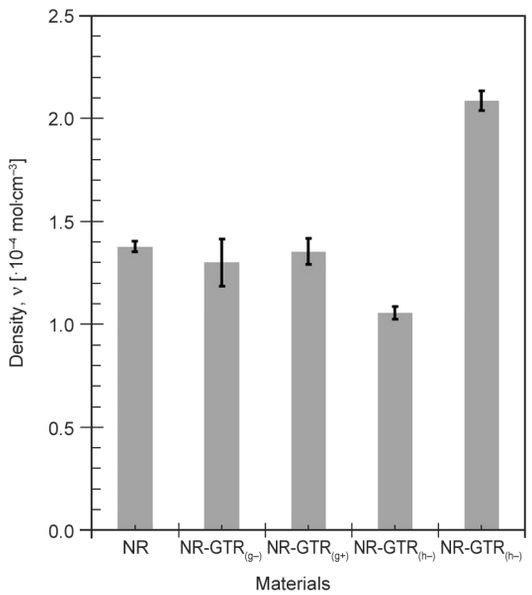

Figure 6. Network chain density of NR, NR/GTR$_{(g-)}$, NR/GTR$_{(g+)}$, NR/GTR$_{(h-)}$ and NR/GTR$_{(h+)}$. The symbols – and + indicate the quantity of crosslinking agent (DCP) introduced (see Table 1).

when compared with NR/GTR$_{(g)}$. One explanation may be that migration of DCP from the NR matrix to wastes and/or migration from the remaining sulphur system from the GTR (from tire curing) to the NR matrix occurs. One may state indeed that large waste particles (obtained from HSM) limit the mutual migration of sulphur and DCP, owing to the lower surface area between the two phases (NR and GTR), hence promoting the formation of crosslinks. This apparent high reactivity of the NR/GTR$_{(h)}$ blend with DCP is consistent with the large increase of torque seen during the MDR curing curve (Figure 1) as well as the elevated elastic modulus in DMA experiments (Figure 2). Such drastic changes in the network chain density of the NR/GTR are expected to impact the large strain tensile properties, such as strain-induced crystallization abilities, as studied in the following section.

3.2. Tensile and strain-induced crystallization properties

Tensile properties of the NR/GTR blends using wastes obtained after grinding or after HSM processes were compared. Our vulcanized NR material shows hyperelastic behaviour with reinforcement at large strain, as seen in Figure 7a, which is usually ascribed to its ability to crystallize under strain. Even if the crystalline fraction in the NR remains minor (generally less than 20–25 vol.%), the high stiffness and orientation of the crystalline domains are known to reinforce the stress in the tensile direction, acting as temporary fillers.

One important usage of waste rubber for pneumatic tyre (GTR) in fresh rubber matrices relates to their mechanical reinforcement abilities. NR/GTR blends show similar tensile behaviour as compared to NR (Figures 7b, 7c). The tensile and strain-induced crystallization (SIC) properties of the NR and NR/GTR blends are shown in Figure 8. The elastic modulus – calculated by using the gaussian approximation [32] – has been found to slightly increase with the applied strain rate for all NR and NR/GTR blends (Figure 8a). Assuming a time-temperature equivalence in the elastic strain regime, an increase of the strain rate limits chains relaxation, and hence induces a higher chains stiffness. Possibly, more trapping of chains entanglements may occur with high strain rate, that also contributes to the increase of the elastic modulus (Figure 8a).

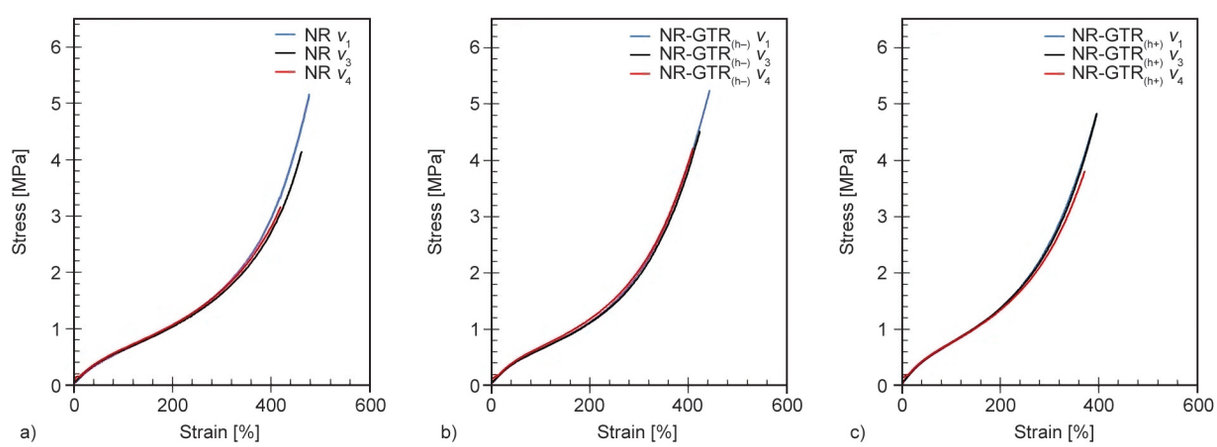

Figure 7. Room temperature tensile curves of NR (a), NR/GTR$_{(h-)}$ (b) and NR/GTR$_{(h+)}$ (c) blends for various strain rates of v_1 = 1.1 %/s, v_3 = 11 %/s and v_4 = 222 %/s.

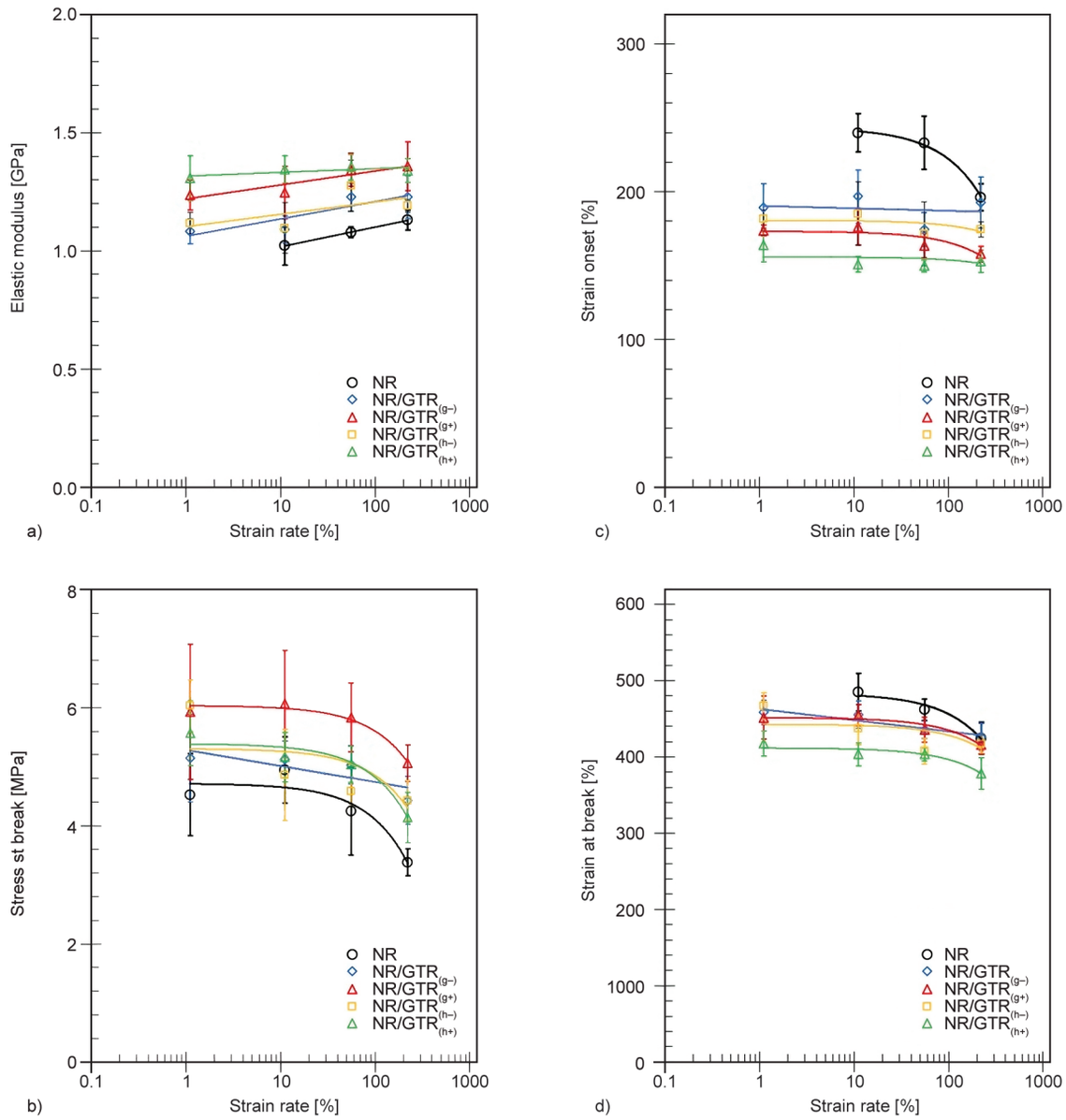

Figure 8. Room temperature tensile parameters of NR and NR/GTR blends as a function of the strain rate from 1.1, to 222 %/s: a) Elastic modulus, b) strain at crystallization onset, c) stress at break and d) strain at break.

The strain at crystallization onset estimates the appearance of the incipient strain induced crystals. It is used here to measure the possible effect of the waste particles on the improvement of SIC in the NR matrix. It has been suggested in previous works [18], that the deviation of the tensile behaviour from the gaussian approximation may be ascribed to the initiation of the strain induced crystalline phase that causes a large strain reinforcement. Such statement had been proven by direct characterization method of SIC such as the *in-situ* X-rays [17]. We applied the method used in that previous works to identify the strain at crystallization onset (Figure 8b). Only weak effect of the strain rate is observed, except for the pure vulcanized NR that tends to show a decrease of the strain onset with strain rate. Stress at break (Figure 8c) is found to decrease for the highest strain rates studied (above 100 %/s), concomitantly with a decrease of the strain at break (Figure 8d). In such high strain rate conditions of solicitation, the presence of highly oriented crystals in NR and NR/GTR, combined with the presence of waste rubber as reinforcing fillers, may contribute to the increased local strain in the amorphous part of the NR matrix, hence causing a premature failure.

The tensile and strain-induced crystallization parameters were discussed for the highest strain rate studied (Figure 9), where possible applications can be found, such as the elastocaloric effect due to the generation of heating/cooling induced by crystallization/

melting processes near adiabatic conditions [18]. The effect of the presence of waste rubber on the tensile properties of rubber blends has been considered in the literature [33], where the presence of carbon black in the waste particles had been evoked to partly explain a mechanical reinforcement effect. The elastic modulus is found to decrease from NR to NR/GTR blends when lower DCP quantity is used but is found to increase from NR to NR/GTR blends when higher DCP quantity is used (Figure 9a), consistent with differences in the crosslink densities (Figure 5). Our results are consistent with the literature where the elastic modulus of rubber is increased in the presence of waste fillers [34]. In prior works, it has been shown that the property of the natural rubber matrix to crystallize under strain could be improved by the presence of waste rubber [17]. The latter are playing the role of nucleating agents for SIC, by amplifying the local deformation in the NR matrix. In this study, this nucleating effect is shown for the two types of NR/GTR blends: in both cases, the higher the quantity of crosslinking agent, the lower the strain onset (Figure 9b). It has been shown in the literature that the strain at crystallization onset decreases while increasing the network chain density in a range between 0.76 and $1.93 \cdot 10^{-4}$ mol·cm^{-3} [35] for peroxide-cured NR. The higher the network chain density, the higher the chains alignment and the orientation along the stretching axis, favouring the occurrence of SIC. Our results do not show clear

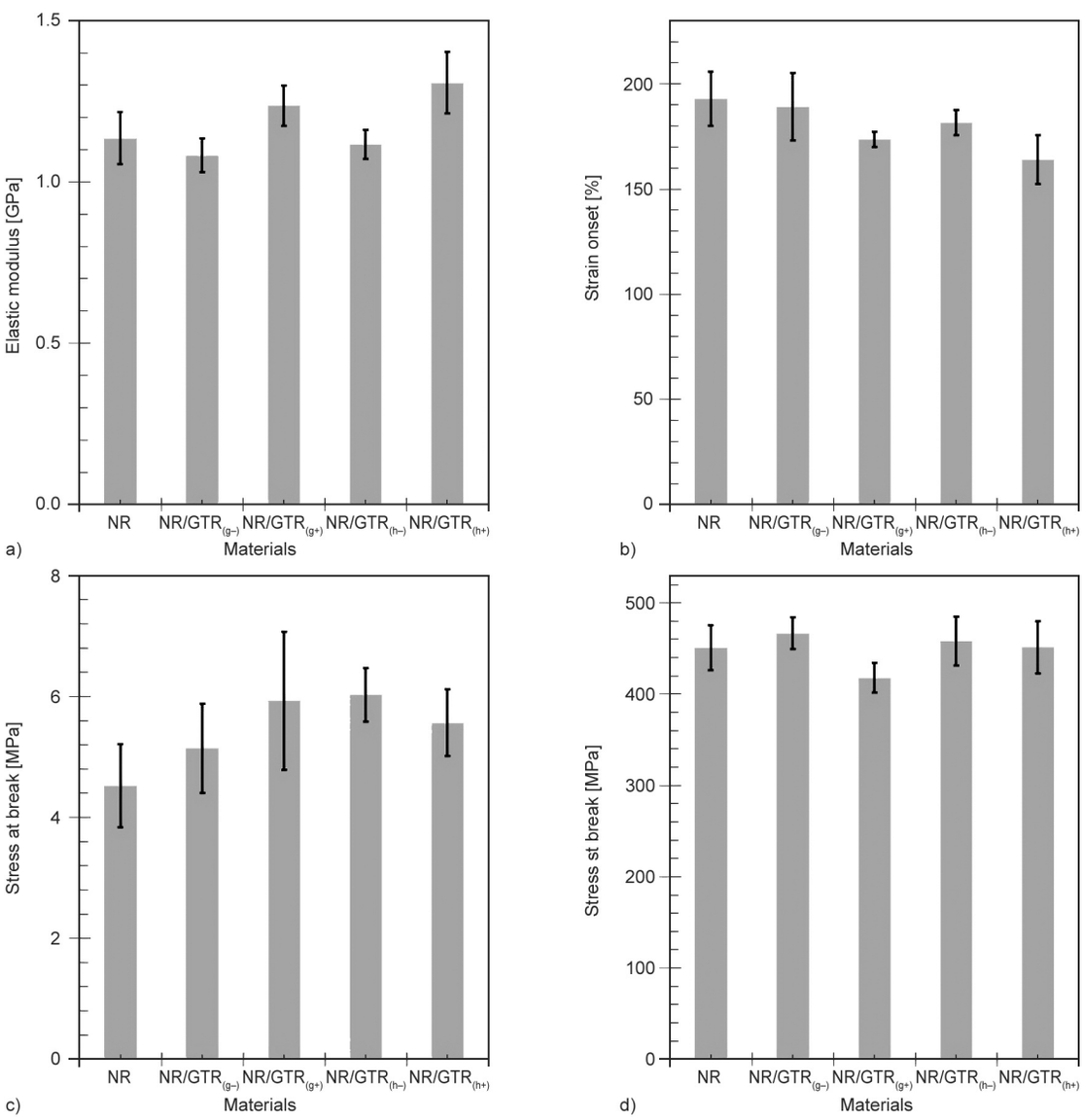

Figure 9. Mechanical parameters measured during tensile experiments performed at 21 °C and at the strain rate v_4 = 222 %/s: a) elastic modulus obtained from the Gaussian approximation, b) strain at crystallization onset estimated from the deviation of the tensile curve from the Gaussian approximation, c) stress at break and d) strain at break.

correlation between the network chain density and the strain at crystallization onset. Nonetheless, in our system, a better representation of the chains orientation is the elastic modulus (Figure 9a), as it considers both chemical crosslinks and entanglements trapped during the tensile test. The higher the elastic modulus, the lower is the strain at crystallization onset. The stress at break is found to increase in presence of GTR, likely due to both the reinforcement effect of the carbon black particles in the wastes but also owing the nucleation ability of theses wastes to favour SIC (Figure 9c). One may note that in the case of NR/GTR$_{(h+)}$ blends, tensile properties are decreased. This can be attributed to a higher quantity of cavitation originated at NR-GTR interface that may participate in materials softening, especially at such high strain rate conditions (222 %/s), favoured by the presence of larger waste particles obtained from HSM process (see Figure 1). Such correlation between stress softening and the occurrence of cavitation had been studied previously in filled EPDM in the same strain rate range [36]. The strain at break does not seem to be widely influenced by the presence of wastes, nor by the type of waste processing (Figure 9d).

The environment temperature is known to widely influence the strain-induced crystallization behaviour of NR materials and hence influence its associated mechanical reinforcement. Tensile tests carried out on NR and NR/GTR specimens at a given strain rate (v_2 = 11 %/s) and at various temperatures show hyperelastic behaviour with reinforcement at large strain (Figure 10). The latter is more pronounced when decreasing the temperature. This is likely ascribed to the promotion of SIC ability while decreasing the temperature in the same temperature range, as shown in the literature [37, 38].

Elastic moduli are not found to be dependent on the temperature in the temperature range studied (Figure 11a). Nonetheless, the strain at crystallization onset is found to increase with the temperature (Figure 11b). It has been shown in the literature that –25 °C is the optimum temperature for thermal crystallization in both vulcanized NR and NR containing reinforcing fillers (carbon black or silica) [39] due to competition – at temperatures between the glass transition temperature and the melting temperature – between crystal nucleation (activated at low temperature) and molecular diffusion to make a crystal growing (activated at high temperature). It has also been shown that this optimum is between –25 and –10 °C when combined with thermal and strain-induced crystallization in the strain range of the present paper [40]. Our results obtained about the strain at crystallization onset reveal the same dependence on the temperature for both NR and NR/GTR. Interestingly, the addition of GTR into the NR matrix seems to slightly increase the optimum temperature of crystallization in comparison with pure NR. This shift is expected to occur when increasing the strain rate, as demonstrated by both experiments and physical modelling [40]. In the case of our blends, the presence of GTR fillers increases the local deformation in the crystallizing NR matrix, as well as its local strain rate, compared to the strain rate in the neat NR. As the strain rate is increased, the nucleation is forced to occur at higher strain, and the contribution of the nucleation term (driven by entropy force) is predominant and tends to shift the optimum temperature to higher values (see reference [40] for a detailed

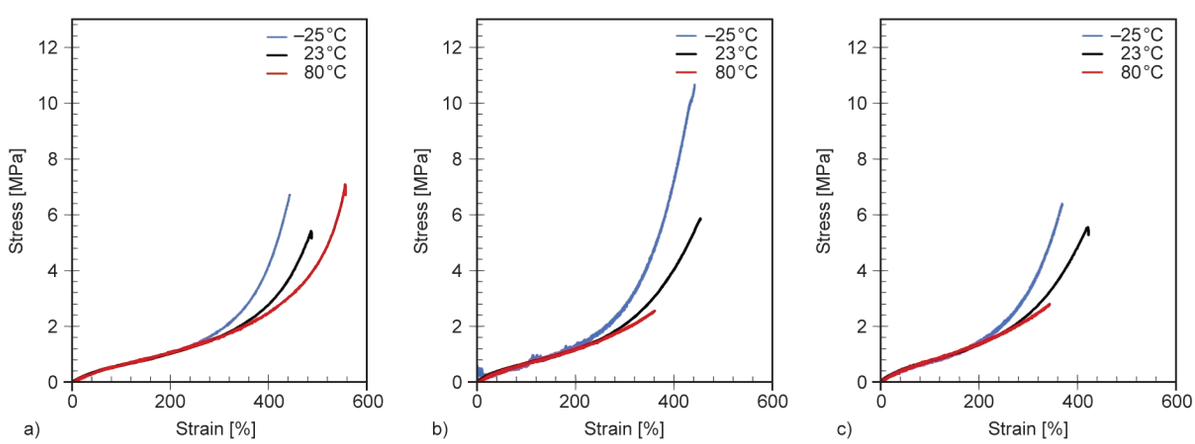

Figure 10. Tensile curves of NR (a), NR/GTR$_{(h-)}$ (b) and NR/GTR$_{(h+)}$ (c) at the strain rate of v_2 = 11 %/s and at various temperatures: –25, 23 and 80 °C.

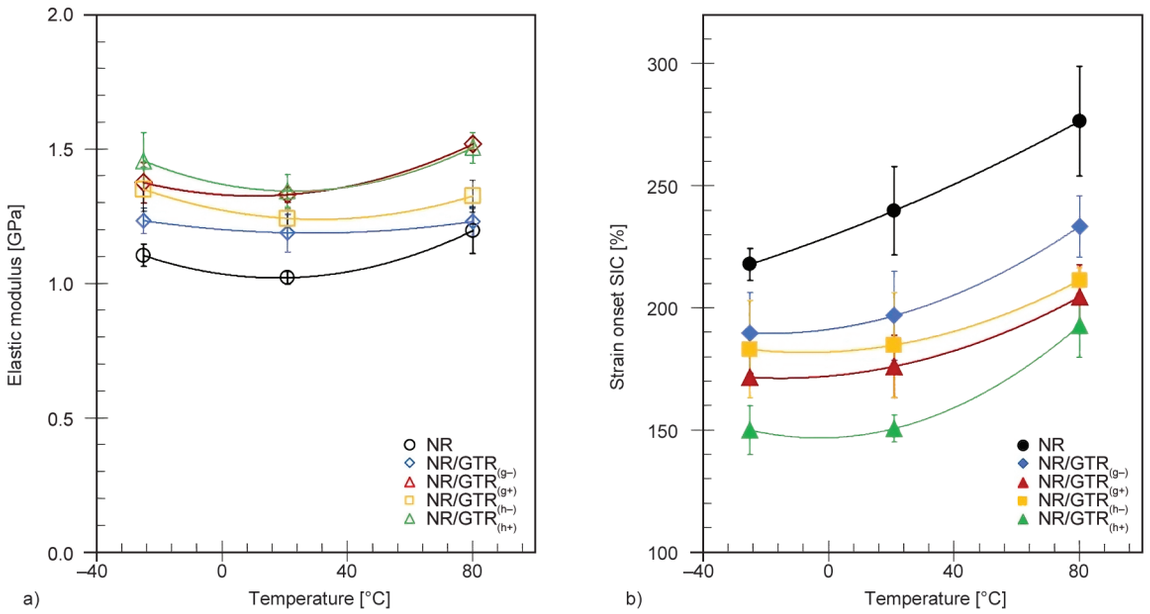

Figure 11. Elastic modulus (a) and strain at crystallization (b) onset of NR and NR/GTR blends at the strain rate of v_2 = 11 %/s and at various temperatures: –25, 21 and 80 °C.

demonstration). One interesting application is the possibility of these NR/GTR blends to operate in an optimum way (*i.e.*, when SIC occurs at the lowest strain) at a temperature close to room temperature. It may be useful for applications requiring SIC to occur at high strain rates, such as heating/cooling systems using the elastocaloric effect in NR, that may operate with usual temperatures close to 21 °C in countries with a temperate climate.

The effect of the GTR on elastic modulus and strain at crystallization onset are illustrated for the series of tensile tests at –25 °C (Figure 12). The presence of GTR is found to increase the blend's stiffness. One may note that the reinforcing effect of the GTR on the elastic modulus is more important at low temperatures (Figure 12a), in comparison with the results obtained at room temperature (Figure 9a). Similarly, the effect of the GTR on the strain at crystallization onset is more visible. The presence of GTR decreases the strain at crystallization onset, and the higher the crosslink density of the NR/GTR, the lower the strain at crystallization onset for the two types of

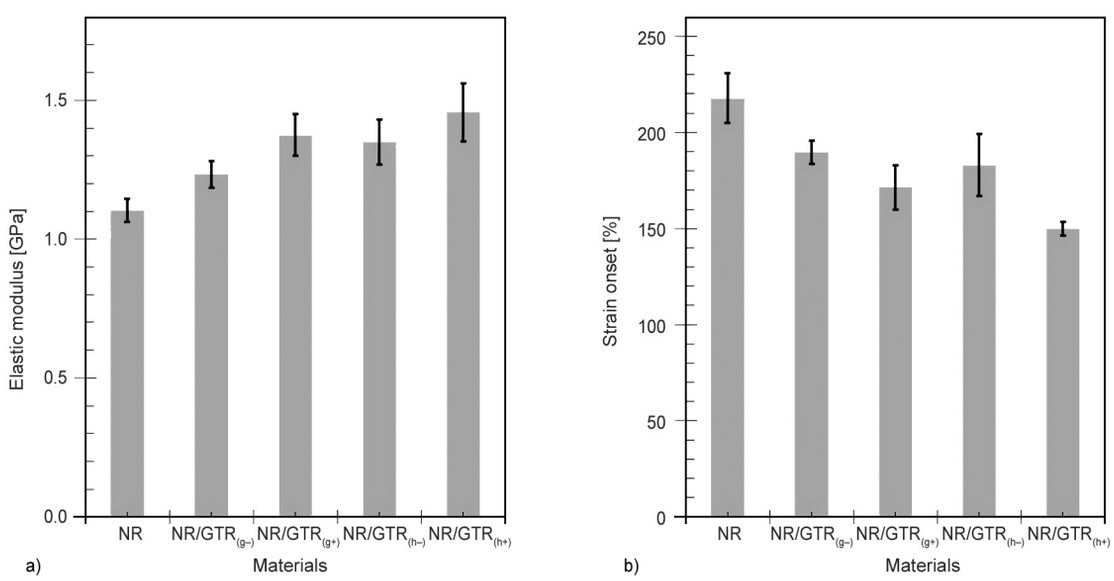

Figure 12. Mechanical parameters were measured during tensile experiments performed at –25 °C and at the strain rate v_2 = 11 %/s: a) elastic modulus obtained from the Gaussian approximation, b) strain at crystallization onset estimated from the deviation of the tensile curve from the Gaussian approximation.

NR/GTR. Such conclusions are similar to previous results observed at 21 °C and at the strain rate v_4 = 222 %/s (Figure 9c, Figure 9d). Moreover, the NR/GTR blends containing GTR particles obtained with HSM ($GTR_{(h)}$) show the highest elastic modulus. This result is consistent with the literature that shows that the elastic modulus of rubber blends using waste latex is increased while increasing the waste diameter, while the finest diameters are closer to the theoretical expectations from the Einstein equation [41]. Consistent with such an increase of elastic modulus, SIC onset is found to appear at the lowest strain for $NR/GTR_{(h)}$, confirming a trend seen from results at 21 °C and at the strain rate v_4 = 222 %/s (Figure 9a, Figure 9b).

Until now, single tensile loading had been applied on the NR and NR/GTR blends. To make the NR/GTR blends suitable for industrial applications, the cyclic behaviour must be investigated. High strain rate strain-induced crystallization may indeed generate an elastocaloric effect that can be used for heating/cooling devices working under cyclic loading to generate continuous heating and/or cooling with operating time. In the present paper, a series of incremental tests were performed (see Table 2 for the testing conditions). The loading conditions and the evolution of the stress-strain behaviour in such type of experiments is illustrated for the $NR/GTR_{(h+)}$ in Figure 13. The first cycles show hyperelasticity and reversibility with the absence of mechanical hysteresis. However, from an applied deformation at and above 300%, the cycles induce a dissipation of the mechanical energy that is most likely due to the occurrence of SIC.

Such energy dissipation is considered as a signature of SIC. It is calculated from the area of the mechanical cycle and express in $MJ \cdot m^{-3}$ (or equivalently in MPa). The detailed procedure for the estimate of such energy dissipation is given in reference [18]. When potted against the maximum applied strain, it results in a progressive increase that directly related to the progressive building of the crystalline domains upon deformation (Figure 14). In such cyclic conditions, once again, the presence of GTR is found to act as nucleating agent for SIC. The higher the crosslink density for the NR/GTR blends, the more pronounced is the nucleating effect for both types of NR/GTR using different varieties of waste rubber treatments.

In a last series of tests, the NR and NR/GTR blend are studied by applying continuous cycles of an amplitude of 200% after the application of a pre-deformation of 400%. Such conditions are expected to generate strain-induced crystallization during loading and full melting during unloading, hence associated with mechanical dissipation. In all samples, both maximum stress (Figure 15a) and dissipated energy (Figure 15b) are found to decrease with the number of cycles. The drastic decrease in the dissipated energy within the first cycles is likely due to the decrease in the crystallization/melting abilities. This is particularly true for the NR/GTR blends, especially

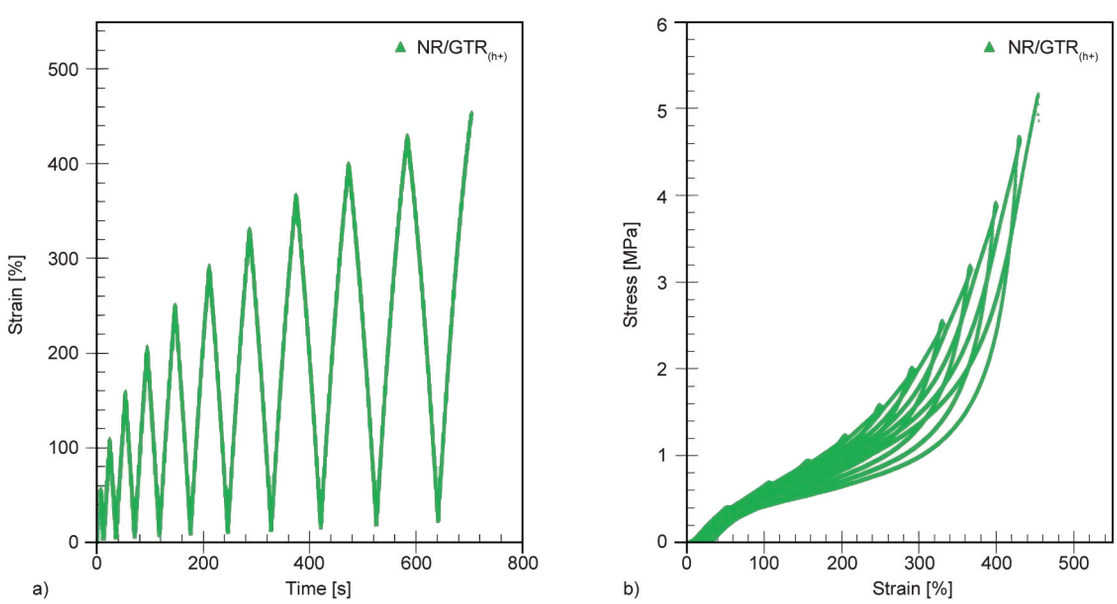

Figure 13. Cyclic loading of the $NR/GTR_{(h+)}$ during incremental tests (a) and stress-strain behaviour during such type of test (b).

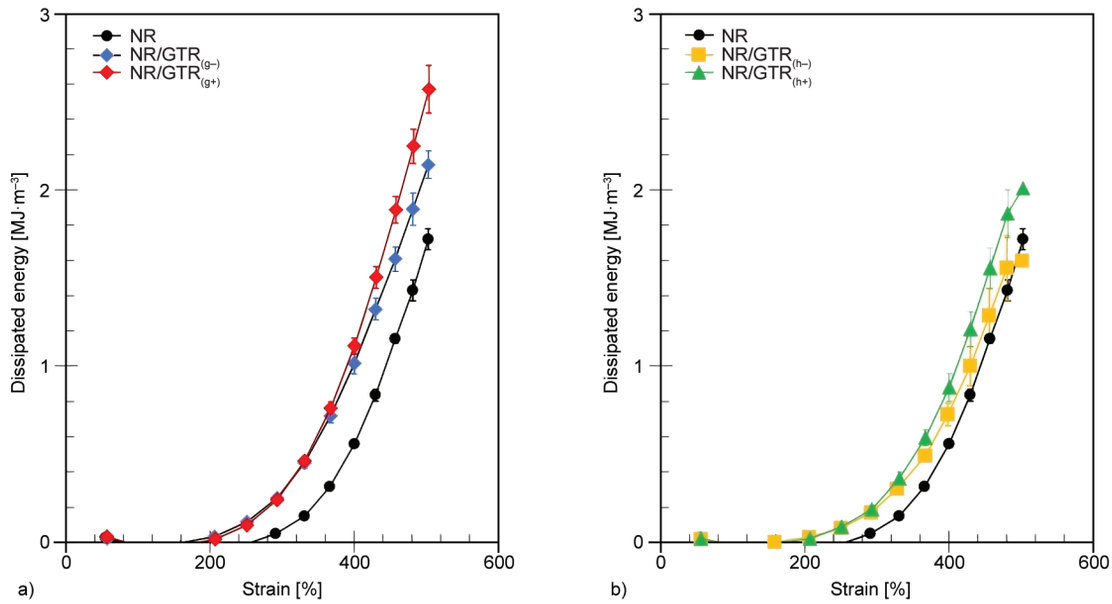

Figure 14. Evolution of the dissipated energy *versus* strain during incremental cycles for a) NR/GTR blends using cryoground GTR compared with neat NR and for b) NR/GTR blends using GTR passed through HSM process compared with neat NR.

those with higher network chain densities. In such types of experiments, a memory effect of the strain-induced crystals may cause the persistence of a fraction of the crystalline phase after unloading, as had been demonstrated in vulcanized NR [42]. This likely results in a decrease of the energy dissipation associated with its further crystallization/melting in subsequent cycles. After the application of hundreds of cycles, the NR/GTR blends with the highest network chain density show the best ability to dissipate mechanical energy, with the highest value obtained for the blends using cryoground GTR ($GTR_{(g)}$). Such ability may be related to the fact that the blends containing the finest GTR particles, independently of the quality of the NR/GTR interface, possibly faceless cavitation, and better distribute the stress in the NR matrix. These results suggest these blends be interesting materials for potential elastocaloric properties while working into heating/cooling devices, owing to their possible ability to continuously

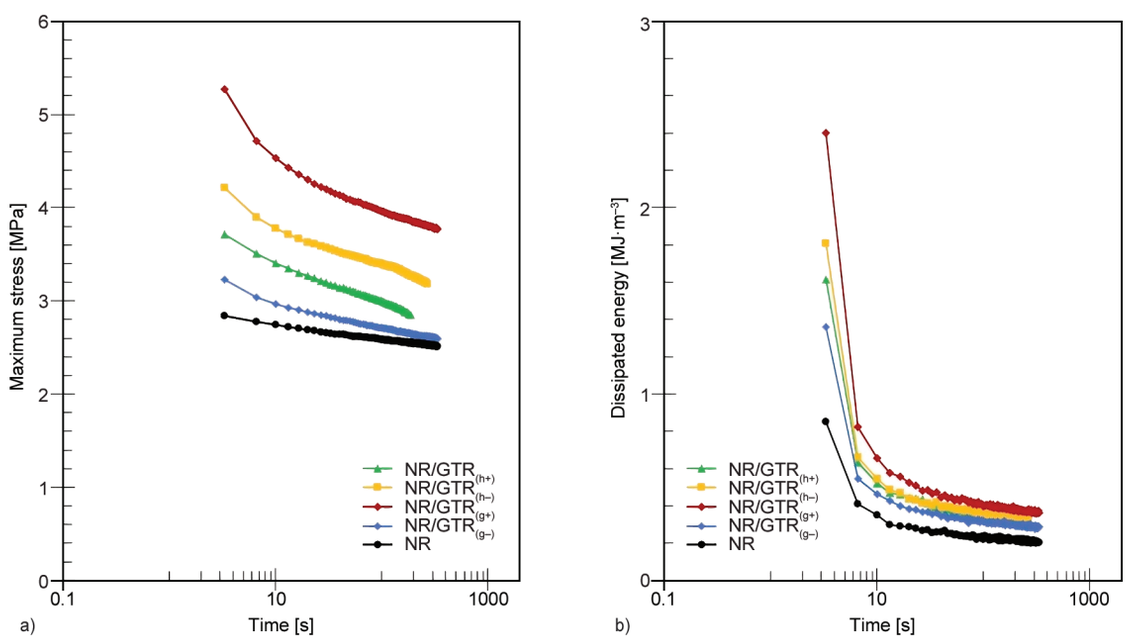

Figure 15. Maximum stress was measured during the cyclic tests at a strain rate of 120 %/s. A pre-deformation of 400% has been applied followed by a cyclic test with a strain amplitude of 200%: a) maximum stress, b) dissipated energy

generate heat and cool during repetitive mechanical cycles.

4. Conclusions

We have prepared peroxide-cured waste/natural rubber blends by internal mixer and by hot press. These blends contained a natural rubber matrix and waste rubber from the pneumatic industry (ground tyre rubber) that were obtained by two distinct mechanical recycling processes: $GTR_{(g)}$ by cryo-grinding and $GTR_{(h)}$ by high shear mixing process. On one side, it has been shown that the cryo-grinding process resulted in the obtention of the finest particles, as demonstrated by μCT. On the other side, rheology and dynamic mechanical analysis performed on GTR powder obtained from HSM and on NR/GTR blend revealed an elastic response that suggests the formation of interfacial strength between the GTR particles and between the GTR particles and the NR matrix as compared to the blend using cryoground particles. The tensile properties of NR/GTR blends using both types of GTR treatment were investigated under several conditions by varying the tensile speed (from 1.1 to 222 %/s), the specimen temperature (from -25 to 80 °C) and the mechanical path (single cyclic loading or incremental cycles). It has been shown that owing to the highest degree of crosslinking in the NR/GTR using GTR obtained from HSM, the elastic modulus was the highest, and the strain at crystallization onset was the lowest during single tensile loading. Contrarily, in more drastic conditions of solicitation, such as cyclic loadings, the NR/GTR blends using cryoground GTR show the highest tensile properties as well as a higher capacity to generate strain-induced crystallization. This suggests a better accommodation of the strain in such types of blends (less molecular scale damage such as crosslinks breakage, chains scission, or less decohesion at NR/GTR interface). The results suggest that the HSM is a promising process for waste rubber recycling to enhance the tensile properties of NR but shows a limitation under cyclic conditions due to possible damage of the material due to (i) a to high level of crosslinks and/or (ii) the loss of the interfacial strength after the application of a series of cycle due to too a strong localization of the stress because of the large size of the waste particles. A possible improvement would consist in combining cryo-grinding and HSM processes to use the advantage of both techniques: size reduction from cryo-grinding and higher interfacial strength from the HSM. Finally, the measure of the devulcanization state of the GTR, especially from the HSM process, by using swelling and Soxhlet extraction, would be of great interest to optimize the re-vulcanization process.

Acknowledgements

N. Candau acknowledges the Spanish Ministry of Science and Innovation (Project TED2021-129952A-C33, and the group eb-POLICOM/Polímers i Compòsits Ecològics i Biodegradables, a research group of the Generalitat de Catalunya (Grant 2021 SGR 01042). We acknowledge Rodrigo Diaz-Vargas from the REP-International company, for performing the high shear mixing process as well as the curing experiments carried out on the waste rubber.

References

[1] European Comission: European strategy for market development of innovative use of tyre recycled materials. (2023).

[2] Mohajerani A. Burnett L., Smith J. V., Markovski S., Rodwell G., Rahman M. T., Kurmus H., Mirzababaei M., Arulrajah A., Horpibulsuk S., Maghool F.: Recycling waste rubber tyres in construction materials and associated environmental considerations: A review. Resources, Conservation and Recycling, **155**, 104679 (2020). https://doi.org/10.1016/j.resconrec.2020.104679

[3] European Commission: Recycling technology to introduce rubber from end-of-life tyres into production lines as virgin rubbers substitute. (2023).

[4] Shu X., Huang B.: Recycling of waste tire rubber in asphalt and portland cement concrete: An overview. Construction and Building Materials, **67**, 217–224 (2014). https://doi.org/10.1016/j.conbuildmat.2013.11.027

[5] Goto M.: Chemical recycling of plastics using sub- and supercritical fluids. Journal of Supercritical Fluids, **47**, 500–507 (2009). https://doi.org/10.1016/j.supflu.2008.10.011

[6] de Sousa F. D. B., Scuracchio C. H., Hu G-H., Hoppe S.: Devulcanization of waste tire rubber by microwaves. Polymer Degradation and Stability, **138**, 169–181 (2017). https://doi.org/10.1016/j.polymdegradstab.2017.03.008

[7] Arabiourrutia M., Lopez G., Artetxe M., Alvarez J., Bilbao J., Olazar M.: Waste tyre valorization by catalytic pyrolysis – A review. Renewable and Sustainable Energy Reviews, **129** 109932 (2020). https://doi.org/10.1016/j.rser.2020.109932

[8] Junghare H., Hamjade M., Patil C., Girase S. B., Lele M. M.: A review on cryogenic grinding. International Journal of Current Engineering and Technology, **7**, 420–423 (2017).

[9] Hrdlička Z., Hrdlička Z., Brejcha J., Šubrt J., Vrtiška D., Malinová L., Čadek D., Kadeřábková A.: Ground tyre rubber produced *via* ambient, cryogenic, and waterjet milling: The influence of milling method and particle size on the properties of SBR/NR/BR compounds for agricultural tyre treads. Plastics, Rubber and Composites, **51**, 497–506 (2022). https://doi.org/10.1080/14658011.2021.2008713

[10] Diaz R., Colomines G., Peuvrel-Disdier E., Deterre R.: Thermo-mechanical recycling of rubber: Relationship between material properties and specific mechanical energy. Journal of Materials Processing Technology, **252**, 454–468 (2018). https://doi.org/10.1016/j.jmatprotec.2017.10.014

[11] Zhang X-X., Lu C-H., Liang M.: Preparation of rubber composites from ground tire rubber reinforced with waste-tire fiber through mechanical milling. Journal of Applied Polymer Science, **103**, 4087–4094 (2007). https://doi.org/10.1002/app.25510

[12] Karger-Kocsis J., Mészáros L., Bárány T.: Ground tyre rubber (GTR) in thermoplastics, thermosets, and rubbers. Journal of Materials Science, **48**, 1–38 (2013). https://doi.org/10.1007/s10853-012-6564-2

[13] Roychand R., Gravina R. J., Zhuge Y., Ma X., Youssf O., Mills J. E.: A comprehensive review on the mechanical properties of waste tire rubber concrete. Construction and Building Materials, **237**, 117651 (2020). https://doi.org/10.1016/j.conbuildmat.2019.117651

[14] De D., Panda P. K., Roy M., Bhunia S.: Reinforcing effect of reclaim rubber on natural rubber/polybutadiene rubber blends. Materials and Design, **46**, 142–150 (2013). https://doi.org/10.1016/j.matdes.2012.10.014

[15] Barrera C. S., Cornish K.: High performance waste-derived filler/carbon black reinforced guayule natural rubber composites. Industrial Crops and Products, **86**, 132–142 (2016). https://doi.org/10.1016/j.indcrop.2016.03.021

[16] Chandran V., Nagarajan L., Thomas M. R.: Evaluation of vibration damping behavior of different sizes of waste tyre rubber in natural rubber composites. Journal of Composite Materials, **52**, 2493–2501 (2018). https://doi.org/10.1177/0021998317748467

[17] Candau N., Oguz O., Federico C. E., Stoclet G., Tahon J-F., Maspoch M. L.: Strain induced crystallization in vulcanized natural rubber containing ground tire rubber particles with reinforcement and nucleation abilities. Polymer Testing, **101**, 107313 (2021). https://doi.org/10.1016/j.polymertesting.2021.107313

[18] Candau N., Vives E., Fernández A. I., Maspoch M. L.: Elastocaloric effect in vulcanized natural rubber and natural/wastes rubber blends. Polymer, **236**, 124309 (2021). https://doi.org/10.1016/j.polymer.2021.124309

[19] Candau N., Vives E., Fernández A. I., Oguz O., Corvec G., Federico C. E., Fernandes J. P. C., Stoclet G., Maspoch M. L.: Observation of heterogeneities in elastocaloric natural/wastes rubber composites. Express Polymer Letters, **16**, 1331–1347 (2022). https://doi.org/10.3144/expresspolymlett.2022.96

[20] Flory P. J., Rehner J.: Statistical mechanics of cross-linked polymer networks II. Swelling. Journal of Chemical Physics, **11**, 521–526 (1943). https://doi.org/10.1063/1.1723792

[21] Sheehan C. J., Bisio A. L.: Polymer/solvent interaction parameters. Rubber Chemistry and Technology, **39**, 149–192 (1966). https://doi.org/10.5254/1.3544827

[22] Kraus G.: Swelling of filler-reinforced vulcanizates. Journal of Applied Polymer Science, **7**, 861–871 (1963). https://doi.org/10.1002/app.1963.070070306

[23] Vieyres A.: Influence of filler/polymer interface on reinforcement, strain-induced crystallization and tear resistance in reinforced natural rubber. PhD These, Ecole Doctorale Matériaux de Lyon (2013).

[24] Robertson C. G., Hardman N. J.: Nature of carbon black reinforcement of rubber: Perspective on the original polymer nanocomposite. Polymers, **13**, 538 (2021). https://doi.org/10.3390/polym13040538

[25] Fernández-Berridi M. J., González N., Mugica A., Bernicot C.: Pyrolysis-FTIR and TGA techniques as tools in the characterization of blends of natural rubber and SBR. Thermochimica Acta, **444**, 65–70 (2006). https://doi.org/10.1016/j.tca.2006.02.027

[26] Liu X., Liu X., Hu Y.: Investigation of the thermal decomposition of talc. Clays and Clay Minerals, **62**, 137–144 (2014). https://doi.org/10.1346/ccmn.2014.0620206

[27] Thitithammawong A., Uthaipan N., Rungvichaniwat A.: The influence of mixed conventional sulfur/peroxide vulcanization systems on the mechanical and thermal properties of natural rubber/polypropylene blends. Journal of Elastomers and Plastics, **44**, 419–432 (2012). https://doi.org/10.1177/0095244311432781

[28] Candau N., Oguz O., Albiter N. L., Förster G., Maspoch M. L.: Poly(lactic acid)/ground tire rubber blends using peroxide vulcanization. Polymers, **13**, 1496 (2021). https://doi.org/10.3390/polym13091496

[29] Rajan R., Varghese S., George K. E.: Role of coagents in peroxide vulcanization of natural rubber. Rubber Chemistry and Technology, **86**, 488–502 (2013). https://doi.org/10.5254/rct.13.87984

[30] Yahya Y. S. R., Azura A. R., Ahmad Z.: Effect of curing systems on thermal degradation behaviour of natural rubber (SMR CV 60). Journal of Physical Science, **22**, 1–14 (2011).

[31] Litvinov V. M., De P. P.: Spectroscopy of rubbers and rubbery materials. iSmithers Rapra Publishing (2002).

[32] Treloar L. R. G.: The physics of rubber elasticity. Oxford University Press, New York (1975).

[33] Zedler Ł., Przybysz M., Klein M., Saeb M. R., Formela K.: Processing, physico-mechanical and thermal properties of reclaimed GTR and NBR/reclaimed GTR blends as function of various additives. Polymer Degradation and Stability, **143**, 186–195 (2017). https://doi.org/10.1016/j.Polymdegradstab.2017.07.004

[34] Zitzumbo R., Alonso S., Estrada-Monje A., Becerra M. B., Avalos F., Medina-Torres L.: Mechanical properties, dynamic mechanical analysis and molecular cross-linking of GTR/NR re-vulcanized blends. Progress in Rubber, Plastics and Recycling Technology, **38**, 280–294 (2022). https://doi.org/10.1177/14777606221127370

[35] Ikeda Y., Yasuda Y., Hijikata K., Tosaka M., Kohjiya S.: Comparative study on strain-induced crystallization behavior of peroxide cross-linked and sulfur cross-linked natural rubber. Macromolecules, **41**, 5876–5884 (2008). https://doi.org/10.1021/ma800144u

[36] Candau N., Oguz O., Peuvrel-Disdier E., Bouvard J-L., Maspoch M. L., Corvec G., Pradille C., Billon N.: Effect of the strain rate on damage in filled EPDM during single and cyclic loadings. Polymers, **12**, 3021 (2020). https://doi.org/10.3390/polym12123021

[37] Candau N.: Compréhension des mécanismes de cristallisation sous tension des élastomères en conditions quasi-statiques et dynamiques. PhD These, Lyon, INSA (2014).

[38] Xie Z., Sebald G., Guyomar D.: Temperature dependence of the elastocaloric effect in natural rubber. Physics Letters A, **381**, 2112–2116 (2017). https://doi.org/10.1016/j.physleta.2017.02.014

[39] Chenal J. M., Chazeau L., Bomal Y., Gauthier C.: New insights into the cold crystallization of filled natural rubber. Journal of Polymer Science Part B: Polymer Physics, **45**, 955–962 (2007). https://doi.org/10.1002/polb.21105

[40] Candau N., Laghmach R., Chazeau L., Chenal J-M., Gauthier C., Biben T., Munch E.: Influence of strain rate and temperature on the onset of strain induced crystallization in natural rubber. European Polymer Journal, **64**, 244–252 (2015). https://doi.org/10.1016/j.eurpolymj.2015.01.008

[41] Mathew G., Singh R. P., Nair N. R., Thomas S.: Recycling of natural rubber latex waste and its interaction in epoxidised natural rubber. Polymer, **42**, 2137–2165 (2001). https://doi.org/10.1016/S0032-3861(00)00492-4

[42] Candau N., Laghmach R., Chazeau L., Chenal J-M., Gauthier C., Biben T., Munch E.: Strain-induced crystallization of natural rubber and cross-link densities heterogeneities. Macromolecules, **47**, 5815–5824 (2014). https://doi.org/10.1021/ma5006843